Part I

Advances in Localized Electrical Testing

LOW-FREQUENCY SCANNING CAPACITANCE MICROSCOPY

Š. LÁNYI *, M. HRUŠKOVIC **
*Institute of Physics, Slovakian Academy of Sciences, Dúbravská cesta 9, 842 28 Bratislava, Slovakia, lanyi@savba.sk
**Faculty of Electrical Engineering and Information Technology, Slovak University of Technology, Ilkovičova 3, 812 19 Bratislava, Slovakia,

ABSTRACT

The operation principle and main properties of a Scanning Capacitance Microscope (SCM) are described. It is called low-frequency, because in its design typical low-frequency techniques are utilised. The main attention is focused on its lateral resolution, signal-to-noise ratio and the possibility to detect dielectric losses.

Mapping the electrostatic field of a shielded microscope probe was used to calculate the stray capacitance, flux density, sensitivity and contrast obtained on a flat conducting surface, as well as on a surface covered by a thin dielectric film. The effect of dielectric losses, represented by a parallel conductance, on the detected capacitance and the resulting phase shift has been derived.

Using the results of mapping, the requirements on a SCM input stage and the possible solutions are discussed. From the point of view of frequency range and noise the best is an electrometric input stage, with input impedance represented by its capacitance.

The achieved signal-to-noise ratio of the low frequency Scanning Capacitance Microscope renders the extension of the working frequency range to lower frequencies. The input stage can be optimised for a frequency range from about 1 kHz to a few MHz, with the possibility to extend it to about 10 MHz at the cost of reduced sensitivity at the lowest frequencies.

INTRODUCTION

The Scanning Capacitance Microscope, though one of the first scanning probe microscopes [1] is among the less known and less used arts of scanning probe techniques. In the last few years its importance has been recognised in connection with the needs of the semiconductor industry, which is in search of high-resolution analytical tools for the next generation of integrated circuits [2]. The main advantage of SCM for such purposes is the ability to image not only conducting surfaces but to sense also the properties of dielectric films or semiconductor depletion layers beneath the surface.

In a SCM the capacitance between a sharp conducting tip and the imaged conducting surface, or a base coated by an insulator, is detected and used to reconstruct its topography. Since the electrostatic field between them is poorly localised, the attainable resolution is lower than can be achieved by scanning tunnelling microscopes (STM) or scanning/atomic force microscopes (SFM, AFM).

In the past three basically different approaches were used to capacitance imaging. The microscopes based on the RCA videodisk pickup [1, 3 - 5] use the change of the resonant frequency of a microstrip resonator, caused by changes of the probe/sample capacitance, connected to it. They operate at about 1 GHz. A similar heterodyne solution, based on a lumped element circuit, was followed in reference [6]. It had a working frequency of 90 MHz. The second possibility was the application of a scanning force microscope, with a charged tip attracted to the surface by Coulomb interaction [7]. The representative of the third concept is the low-frequency capacitance microscope [8], using phase-sensitive demodulation of the ac current flowing through the probe/sample capacitor. Until now it is the only concept that makes the imaging of the

Mat. Res. Soc. Symp. Proc. Vol. 500 © 1998 Materials Research Society

components of the complex capacitance possible. It operates in the MHz region. By means of active shielding of both probe and input stage - a typical low frequency technique - the parasitic stray capacitance of the probe could be significantly reduced. The measurement principle itself helped to separate it from the capacitance of the input of the electronics, also suppressed by bootstrapping. By further modifications the probe/sample capacitance was reduced to a few hundred aF [9].

Recently SCMs became commercially available [10, 11]. They combine the SCM with AFM and use a metal-coated AFM cantilever as SCM probe. This approach makes the separation of contributions of surface topography, detected by AFM, and of inhomogeneity of dielectric film, possible [12].

Most of the important properties, like the lateral resolution, signal-to-noise ratio, etc., strongly depend on the shape of the probe. Its stray capacitance and its dependence on the distance from the probe axis play a crucial role [13]. In this paper we shall present an analysis of a shielded, conical probe with spherical apex. The assumed imaged surface was a conducting plane or a conducting plane covered by an insulating film. The lateral sensitivity to capacitance and to dielectric losses has been derived. The obtained data have been used for a discussion of optimal input stage of the capacitance microscope, designed to work at still lower frequencies.

MAPPING THE ELECTROSTATIC FIELD

The exact calculation of the capacitance between a surface with arbitrary topography and a needle perpendicular to it, is a rather complex problem. It would require the solution of the Laplace equation $\Delta V = 0$ pertinent to the space between electrodes and the electrostatic field at the electrodes, coupled to the charge density through the Poisson equation, with complicated boundary conditions. The problem is further complicated by the local presence of dielectric, properly described by Maxwell's 1st equation. Therefore numerical computation, using the Finite Element Method (FEM), has been used [9, 14]. The employed program [15] is able to calculate the flux and capacitance between electrodes with high accuracy [16].

Four types of arrangements have been solved: i) the whole probe with the shield over a conducting plane, ii) detail of the tip over a conducting plane, iii) both configurations with the conducting plane covered by dielectric films and iv) the same assuming dielectric films with losses. The dependence of capacitance and dielectric losses on increasing distance from the probe axis was estimated by cutting out reduced details of the tip (zooming) and computing their capacitance.

Though we could confirm the high accuracy of the program, nevertheless, it was not sufficient to calculate reliably very small changes of the capacitance if the distance of the whole probe (with actual size of half the axial section 240 µm x 300 µm) from the planar electrode changed by 5 or 10 nm. The change in capacitance was then comparable with the computational errors or effected by possible changes of the automatically generated triangular grid. Therefore, in such cases a thin slice with separately generated grid, of height equal to the change in separation, has been added. Thus the shape of the grid in the rest of the field was retained. In this way the computational error has become a systematic one and minute changes of the order of 10 ppm could be computed. Utilising the rotational symmetry, axial half-sections have been solved.

Boundary conditions

Previous analysis has shown that proper shielding can significantly reduce the stray capacitance of the probe [9]. The experience with the microscope has lead to some modifications. A flat face of the shield with a radius of 0.3 mm, placed a few µm above the sample, was found to

be not convenient [8]. Therefore, the shape of the shield was changed to slightly conical one, with the opening of the orifice just sufficient to let a 0.05 mm diameter wire through. The tip is let to protrude by 5 to 10 μm. This does not increase the stray capacitance significantly, however, the tip may follow also rough surfaces and its adjustment is much easier. The dimensions used in the model correspond to the real probe, except the assumption of spherical apex of the tip. It has frequently a less regular shape and sometimes it is truncated. From the point of view of achieved lateral resolution and contrast, the spherical shape is probably the least advantageous.

The shielding reduces the area, with which the core of the probe interacts, to less than 1/2 of the radius of the hole [9]. Up to about 1/3 of this distance the force lines from a conical tip to a planar electrode were circular arcs, perpendicular to both the tip and the plane. The detailed mapping of the tip took place using the boundary conditions consisting of an equipotential of the tip shape (cone with spherical apex, with radius of curvature 25 nm), a linear Neumann boundary condition (force line) at the axis, an equipotential representing the conducting plane and such an arc-shaped Neumann boundary condition. The circular arc appeared as appropriate up to about 3 μm from the axis.

The real length of the probe is about 10 mm. For mapping only its last 240 μm were considered. The task was defined by the same tip-shaped equipotential, a force line at the probe axis, the conducting plane, circular arc connecting the plane with the outer edge of the shield (Neumann) and the silhouette of the shield as equipotential. In contrast to earlier modelling [9], the shield was connected with the tip rather by means of a linear Neumann boundary condition then directly, to enable independent computation of the flux and capacitance between the tip and the plane, and between the shield and the plane. This modification is without any consequence, since it was already known that there is virtually no electric field in the depth of the probe. Also the presence of the insulation in the shield was neglected [9]. Alternatively, also a larger part of the outer surface was included into the model, which resulted in larger capacitance between the shield and sample but, as expected, without any effect on the tip-to-sample capacitance.

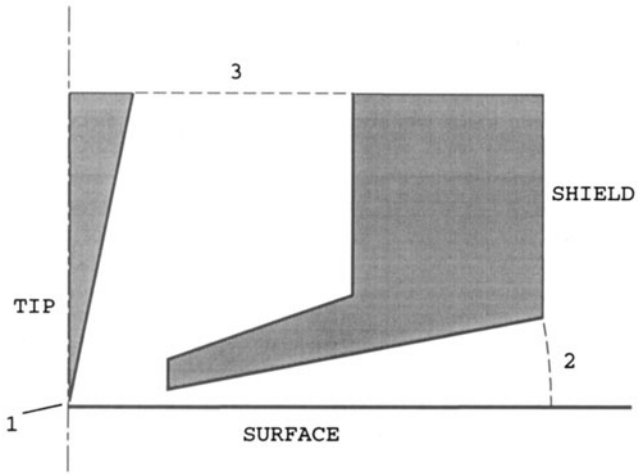

Fig. 1. The boundary conditions used in modelling the shielded probe. 1, 2 and 3 are Neumann boundary conditions.

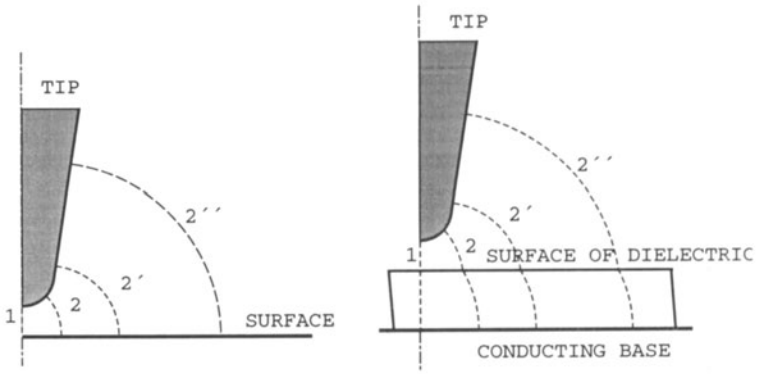

Fig. 2. The boundary conditions used in the modelling of details of the tip. Left: tip over a conducting surface, right: over a dielectric film.

The dielectric film was added as a separate region with relative permittivity $\varepsilon_r = 5$. The assumed thickness was 20, 50, 100 and 200 nm. The correct shape of the Neumann boundary condition at the perimeter is more complex. The force lines are perpendicular to the surface of the tip and to the conducting base, while at the dielectric/air interface only their tangential component is continuous. Therefore the boundary condition consisted of two circular arcs, meeting at the interface under (approximately) proper angles. Sometimes differences in the potential at the dielectric/air interface, have been obtained from sections of different size. They indicated that the boundary conditions were not chosen properly. However, the resulting errors were not significant. The employed boundary conditions are seen in Fig. 1 and 2.

Since a proven way of increasing the lateral resolution is the modulation of the position of the tip perpendicularly to the surface [4, 6, 8], the distance between the tip apex and the surface of the conducting plane or dielectric film was taken 10, 5 and 15 nm. The change of the distance, similarly as the differently thick dielectric films result in changes of spreading of the electric field. To enable comparison of data, the radius r represents the extent of the model at the air/conductor or air/dielectric interface.

The effect of dielectric losses was simulated by assuming the dielectric film to be partly conducting, with conductance equal to its susceptance, resulting in $\tan\delta = 1$. From a given configuration, for which the capacitance was known both without and with dielectric an apparent series capacitance, represented by the film, was calculated. This series capacitor was then replaced with that having dielectric losses and a new capacitance and $\tan\delta$ of the configuration was calculated.

RESULTS OF MAPPING

The accuracy of the method may be tested by comparison of computed results with exact solution of some arrangement, which can be treated analytically. Such tests can be found in reference [16]. Our calculation of the capacitance of a parallel plate capacitor with changing separation of the plates yielded results accurate to at least five digits. The errors appeared to be rounding errors. With more complicated arrangements the errors were up to one order of magnitude larger. Therefore in the cases with dimension ratios 1 to 100, in which relatively uniform grids could be generated, the errors were negligible. Larger sections were divided into

subsections, in which finer grids were used. In this way the accuracy could be increased. In the extreme case of the whole probe, with dimensions ranging from 5 nm, the smallest tip-to-surface distance, up to 240 μm, the considered depth of the probe, the systematic errors resulting from coarser grid could be kept constant, while the fine grid near the tip apex rendered sufficiently exact evaluation of small differences possible.

Conducting surface

The most important property of the probe is the increase of the tip/sample capacitance with increasing radius of the considered sample area. The capacitance between two charged bodies is defined by the ratio C = Q/U, where Q is the induced charge and U the voltage between them. It cannot be really divided into partial capacitors. Therefore, it is more correct to handle the problem of tip/sample capacitance in terms of flux, which can be defined or measured locally.

The results must be evaluated in two ways. With increasing diameter the distance between the tip and the perimeter of the analysed area increases, which results in decreasing contribution of each surface element to the overall capacitance. However, due to the rotational symmetry the affected area increases with the square of radius. As a result, the capacitance increases monotonically up to the limit imposed by the shield. On the other hand, the contribution of a distinct surface element, e.g. an inhomogeneity that would eventually contribute to the contrast, is decreasing with its distance from the tip apex. Fig. 3. shows the capacitance as a function of radius for different tip/sample distances. The limiting values range from 310 to 313 aF. As it was shown in [9], the total capacitance depends on the angle of the tip apex. Nevertheless, the mean features of the analysis remain valid. The capacitance of the analysed part of the shield with respect to the plane is more than two orders of magnitude larger.

The area contributing to the tip/sample capacitance is comparable to or even larger than a typical scanned area. Therefore the integral capacitance will contribute to an image by a mostly featureless background.

An important feature and deficiency of a SCM is the distortion of surface features. Its cause is the long-range Coulomb interaction. Though the same problem exists also in other microscopes for example in AFM or STM, it is much less expressed and can be explained by a convolution of

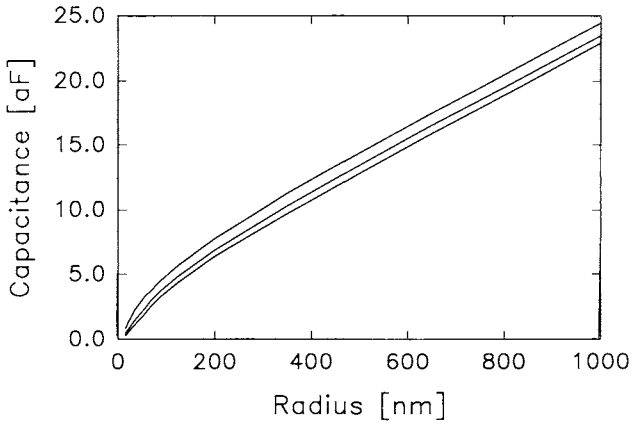

Fig. 3. The increase of the capacitance with the radius of the model. The curves correspond to a tip-to-surface distance of 5 (top), 10 (middle) and 15 nm (bottom).

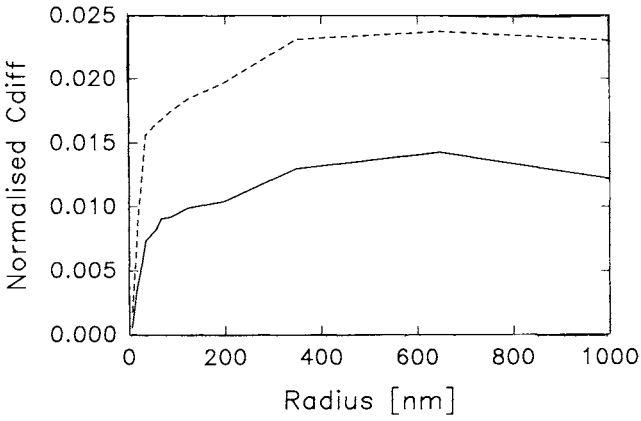

Fig. 4. The differencial capacitance obtained from tip-sample distances 5 nm/10 nm: dashed and 10 nm/15 nm: full

the topography with the tip shape. In an attempt to quantify the imaging ability of SCM we have defined contrast as an objective, measurable property, in analogy with optical imaging. It must not be confused with the contrast of an image, obtained by processing the data. It is understood as the contribution to the signal (capacitance or flux) from areas close to the tip axis, where it is influenced by small-scale inhomogeneities, to the overall capacitance It is then the fraction of the capacitance, seen by a certain part of the probe, i.e. of a circular area with radius r, to the inegral capacitance up to r_{max}. For small radii it would be similar to results in Fig. 3. The contribution to the capacitance is increasing rather slowly.

By changing the probe/sample distance the capacitance *vs.* radius dependences in Fig. 3 are nearly parallel, except at small radii. Their difference divided by d, the difference in probe/sample separation, related to the difference of integral capacitances is seen in Fig. 4. By dividing the data by r the sensitivity, with which a surface element would contribute to the capacitance, can be derived. The result is seen in Fig. 5.

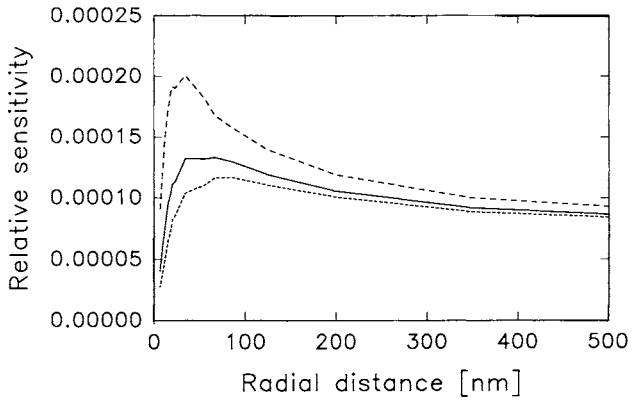

Fig. 5. The lateral sensitivity of the probe

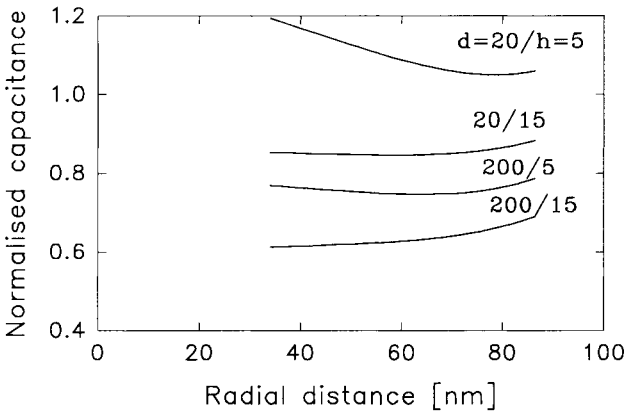

Fig. 6. The local contribution of the dielectric film to the capacitance.

Ideal dielectric film

The evaluation of lateral resolution and contrast in insulating films is more complicated, since due to the three-dimensional geometry of the problem the electric field in them is inhomogeneous. Characterisation of these properties was first attempted in [13]. At present we shall restrict ourselves to the discussion of sensitivity and expected signal-to-noise ratio. Therefore we show only the effect of a dielectric film of certain thickness as a whole. Some data are summarised in Table I. From the results obtained on conducting surface and those on dielectric films an effective series capacitance, represented by the film was calculated. The results are seen in Table II. It is

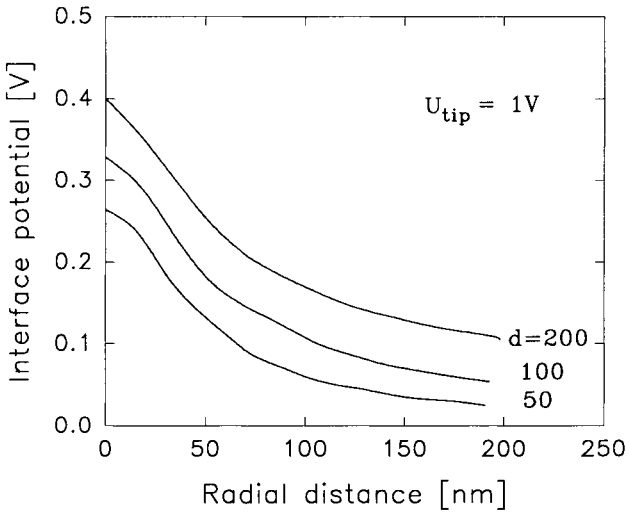

Fig. 7. Potential at the surface of dielectric film.

Dependence of capacitance on the film thickness [aF] TABLE I.

	Dielectric film thickness [nm]				
Radius [nm]	0	20	50	100	200
34	1.484	1.269	1.131	1.031	0.911
67	2.924	2.485	2.266	2.062	1.860
87	3.637	3.219	2.959	2.739	2.509
123	4.723	4.367	4.070	3.803	3.506
198	6.745	6.362	6.030	5.711	5.342
12000	320.122	319.493	316.334	307.980	306.830

interesting to note that for small areas the series capacitance is larger, then it would be for one-dimensional geometry, whereas for the larger areas the opposite is true. It is the result of spreading of the electric field for small *r*, competing with the decrease of the flux density at large radii. As it can be seen in Fig. 6, the local contribution to the decrease of the capacitance may be non-monotonous, which can be explained as a result of a decrease, caused by larger separation from the electrode, partly compensated by the dielectric constant of the film. This point will be discussed in more detail later. The general increase of the contribution of the dielectric film in the vicinity of the probe axis is a result of non-uniform distribution of the applied potential between air and dielectric. The surface potential of the dielectric film is shown in Fig. 7.

Dielectric film with losses

The effect of dielectric losses or non-zero conductivity of the surface film results in a phase shift of the current, sensed by the probe if an ac voltage is connected between the probe and the conducting base. At this point we assume that the phase shift is not influenced in any way by the electronics of the microscope. As already mentioned, we have assumed a $\tan\delta = 1$. This value would be rather high for good dielectrics but still low for many materials, which may become conducting at elevated temperatures. The admittance of the film can be expressed as

$$Y = (1 + i)\,\omega C_s,$$

where $i = \sqrt{-1}$, ω denotes the angular frequency and C_S is the capacitance of the dielectric film. We assume that it is connected in series with the capacitance of the probe, estimated without the film.

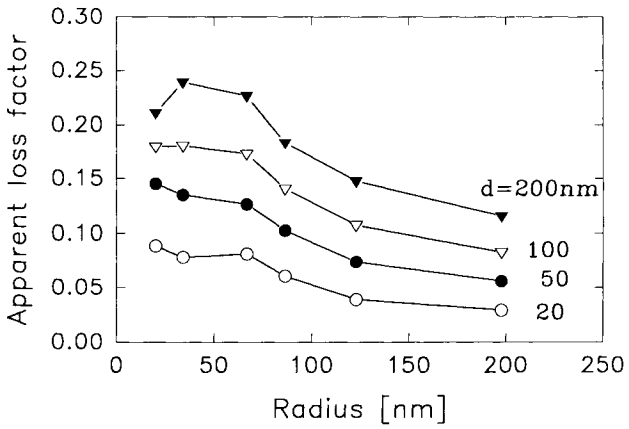

Fig. 8. Radial sensitivity of the probe to dielectric losses.